Physicochem. Probl. Miner. Process., 58(2), 2022, 144375

http://www.journalssystem.com/ppmp

Physicochemical Problems of Mineral Processing

ISSN 1643-1049

Structure of aluminosilicate-supported nickel and iron oxides nanocomposites in gaseous and aqueous media

Olena Goncharuk [1,2,3], Alla Dyachenko [4], Ewa Skwarek [5], Olena Ischenko [4], Lyudmila Andriyko [1,6], Mykola Borysenko [1], Iryna Sulym [1], Dariusz Sternik [5], Klaudia Kowalska [5], Andrii Marynin [6]

[1] Chuiko Institute of Surface Chemistry, NASU, 17 General Naumov str., 03164 Kyiv, Ukraine

[2] Ovcharenko Institute of Biocolloidal Chemistry, NASU, 42 Vernadskii av., 03142 Kyiv, Ukraine

[3] National Technical University of Ukraine «Igor Sikorsky Kyiv Polytechnic Institute», 37 Peremohy av., 03056 Kyiv, Ukraine

[4] Taras Shevchenko National University of Kyiv, 64/13 Volodymyrs'ka str., 01033 Kyiv, Ukraine

[5] Chemistry Department, Maria Curie-Sklodowska University, M. Curie-Sklodowska sq. 3, 20031 Lublin, Poland

[6] National University of Food Technology, 68 Volodymyrs'ka str., 01033 Kyiv, Ukraine

Corresponding author: iscgoncharuk@meta.ua (Olena Goncharuk)

Abstract: A series of mixed oxides was synthesized by deposition of a guest phase on a highly dispersed oxide matrix. Fumed nanooxides SiO_2, Al_2O_3, SiO_2/Al_2O_3, and $SiO_2/Al_2O_3/TiO_2$ with the specific surface area of 65-91 m^2/g were selected as highly dispersed matrices. NiO/Fe_xO_y was deposited as a guest oxide using solvate-stimulated modification of a surface of fumed nanocarriers with nickel nitrate and iron(III) formate and subsequent heat treatment up to 600 °C to form NiO/Fe_xO_y. The aim of this work was to study the influence of the composition and structure of fumed oxide matrices and deposited guest phase on the behavior of the composites in gaseous and aqueous media using XRD, nitrogen adsorption and SEM/EDX, and quasi-elastic light scattering (QELS) methods. The low-temperature nitrogen adsorption isotherms have a sigmoid shape with a narrow hysteresis loop characteristic of mesoporous materials. The specific surface area of composites varies from 65 to 120 m^2/g. SEM data show denser aggregate structure of nanocomposites compared to the initial carriers. The primary particle size was in the 30-60 nm range. According to QELS data, there is a tendency to form aggregates of 100 nm - 10 μm in size in the aqueous media. The XRD method shows that the deposited metal oxides are in the form of crystalline phases of NiO with crystallites of 7-23 nm in size, but the iron oxide reflexes were not identified for NiO-containing composites.

Keywords: oxide nanocomposites, NiO/Fe_xO_y, textural properties, particle size distribution

1. Introduction

In recent decades, the progress in nanotechnologies makes it possible to obtain a wide variety of nanomaterials that have adsorption, catalytic, electronic and magnetic properties that differ significantly from the properties of the corresponding bulk materials (Schmidt et al., 2014; Bhagyaraj et al., 2018). Particular interest has the methods for the preparation of nanosized mixed oxides of transition metals, which demonstrate catalytic properties in various processes due to the presence of Brönsted and Lewis active centres of different strengths on their surface. High dispersity of these oxides and the presence of various active surface sites are of importance for their application as sorbents (Al-Nakib Chowdhury et al., 2010; Wisniewska et al., 2016), heterocatalysts with adjustable set and activity of surface acid/base sites (Arandiyan and Parvari, 2009; Gun'ko et al., 2012; Miao et al., 2018; Tanaka et al., 1996), fillers of polymers (Galaburda et al., 2014; Klonos, Pissis et al., 2016; Klonos, Kulyk et al., 2016), etc. In particular, nickel-based mixed oxides are widely used in catalytic processes such as thermal decomposition of organic compounds (Safdari et al., 2020; J. Li, et al., 2008; W. Wei et al., 2020; Y. Wang et al., 2015) or adsorbents (Ravindhranath et al., 2017; Mashkuri et al., 2017; Mahmoud et al., 2015).

DOI: 10.37190/ppmp/144375

Besides the use of similar materials in the oxide form (for the catalysis), they can be also used as precursors of mixed metal catalysts prepared by reduction in the hydrogen atmosphere. Particular interest has doping of Ni oxide with Fe to enhance the catalytic properties with respect to CO_2 methanation (Dias et al., 2021; Gao et al., 2021; Andersson et al., 2006; Meshkini Far et al., 2018) that could be considered as a promising candidate to substitute the noble-metal catalysts. These compositions could have a higher activity than individual constituents in methanation and they could be utilized to obtain superparamagnetic materials (Rutirawut et al., 2015; Zhang et al., 2018; Irfan et al., 2021).

Most of the methods used to prepare nanoparticles of metal oxides, such as coprecipitation (Deng et al., 2004; Pulimi et al., 2009; Teoh et al., 2012), laser vaporization controlled condensation (Radwan et al., 2007), microemulsions (Han et al., 2009; Han et al., 2004; Palanisamy et al., 2009), sol-gel method (Surca et al., 1996; Wu et al., 2007; Thota et al., 2007), ultrasonic treatment (Lysov et al., 2010), microwave irradiation (Lai et al., 2007), hydrothermal synthesis (Beach et al., 2009; Beach et al., 2008), and low pressure spray pyrolysis (Wang et al., 2004; Lenggoroa et al., 2003), are still limited to laboratory scale due to difficult production conditions or the needs of expensive equipment and reagents. Therefore, a method to produce high quality nanoparticles with high with the ability to industrial production of large amounts and low cost is of importance from a practical point of view.

An effective way to control the morphology and other characteristics of nanoparticles could be based on the synthesis of guest phases at a surface of nanocarriers with a high specific surface area (Ebert et al., 2018; Sulym, Sternik et al., 2016; Bogatyrev et al., 2009; Sulym, Goncharuk et al., 2016; Sulym et al., 2015; Goncharuk et al., 2019). One of the effective ways to enhance the adsorption properties of nanosized oxides is to synthesize mixed oxides of different metals and metalloids that allows one to generate a number of surface Lewis and Brönsted active sites of various strength determining the adsorption activity with respect to different adsorbates. Highly dispersed supports are especially promising to prepare heterogeneous catalysts, whose efficiency depends on the specific surface area and concentration and strength of active surface sites.

Usually, for the synthesis, highly dispersed oxides such as silica and alumina are used as nanocarriers (Iler, 1979; Trueba et al., 2005). Fumed silica is one of the most widely used carriers with a large specific surface area, high thermal stability and chemical resistance (Iler, 1979). Fumed alumina is widely used as a catalyst carrier (Trueba et al., 2005; Pines et al., 1960). The use of mixed aluminosilicas as a substrate has not been adequately studied. As a whole, the morphology and structure of the supports have significant effects on the formation of a deposited phase (Sato et al., 2013; Takei et al., 2011). The surface active sites of the carriers can act as nuclei for the formation of a deposited oxide phase, and their nature and concentration affect the structure of the whole nanocomposite.

Within this work, the effects of the structure of such highly disperse substrates as fumed silica, alumina, silica/alumina, and alumina/silica/titania on the formation of the oxide phase of the mixed NiO/Fe_xO_y oxide, which has great potential in the catalytic process of carbon oxides methanation, as well as the morphology of the composite as a whole.

2. Materials and methods

2.1. Materials

Fumed oxides SiO_2 (A-60), Al_2O_3, SiO_2/Al_2O_3 (SA96), and $Al_2O_3/SiO_2/TiO_2$ (AST1) (Pilot plant of Chuiko Institute of Surface Chemistry, Kalush, Ukraine) with similar values of the specific surface area (S_{BET}) of 65-91 m^2/g (Table 1).

Fumed oxides are composed of spherical-like nonporous nanoparticles (NPNP), whose diameter can be estimated as $d \approx 6/(\rho_0 S_{BET})$, where ρ_0 is the true density of NPNP. Nickel nitrate hexahydrate ($Ni(NO_3)_2 \cdot 6H_2O$, ≥ 98.5 %) and Iron (III) formate ($Fe(CHO_2)_3 \cdot 2H_2O$, 98 %) were purchased from KhimlaborReactive Ltd. (Brovary, Ukraine) and used as precursors to synthesize the oxide composites.

2.1.1. Synthesis of NiO/Fe_xO_y -containing composites

Composites with NiO/Fe_xO_y/fumed oxide (Table 2) were prepared using a method of solvate-stimulated modification of the fumed oxides with Ni nitrate/Fe formate and subjected to thermal

Table 1. Textural characteristics of Al_2O_3, A60, SA96, and AST1 supported Ni/Fe oxides

Sample	S_{BET}, m^2/g	S_{micro}, m^2/g	S_{meso}, m^2/g	S_{macro}, m^2/g	V_{micro}, cm^3/g	V_{meso}, cm^3/g	V_{macro}, cm^3/g	V_p, cm^3/g	$R_{p,V}$ nm
SiO_2	80	32	45	3	0.014	0.13	0.07	0.21	23.9
$NiO/Fe_xO_y/SiO_2$	76	20	48	8	0.010	0.28	0.14	0.44	22.8
Al_2O_3	72	21	50	1	0.010	0.11	0.05	0.17	20.6
$NiO/Fe_xO_y/Al_2O_3$	68	15	50	3	0.007	0.26	0.05	0.32	16.8
SA96	65	21	42	3	0.009	0.10	0.05	0.15	21.7
$NiO/Fe_xO_y/SA96$	62	16	46	0.4	0.009	0.38	0.01	0.39	13.4
AST1	91	26	62	4	0.010	0.14	0.08	0.27	22.5
$NiO/Fe_xO_y/AST1$	119	24	91	4	0.012	0.29	0.09	0.39	16.7

Note: Specific surface area in total (S_{BET}), of nanopores (S_{nano}), mesopores (S_{meso}), macropores (S_{macro}) and pore volumes (V_p, V_{nano}, V_{meso}, V_{macro}) at pore radius $R < 1$ nm, 1 nm < R < 25 nm, and $R > 25$ nm, respectively. $R_{p,V}$ represents the average pore radius.

treatments at 600 °C. The pre-modification of a fumed nanooxide carrier with concentrated solutions of salts of the corresponding metals was performed in 8 cm^3 ceramic ball-mill (ball size 2-3 cm, speed of60 rpm) for 1.5 h. The mill was charged with 20 g of fumed oxide carrier and 10 ml of the aqueous solution of Ni nitrate (34.8 mmol) and Fe formate (9.4 mmol) weighted to obtain certain content in the deposits in the resulting composite. After achieving homogeneity, according to microscopic examination, the resulting mixture was air-dried for 24 h. The dried powder was calcined at 600 °C for 1 h. A feature of the solvate-stimulated modification method is the homogeneous distribution of the solvated salt over the carrier surface. This is required to form nanosized crystallites of the deposited oxide phase by the salt thermolysis upon the calcination at 600 °C.

Table 2. Composition of NiO/Fe_xO_y/fumed oxide nanocomposites

Sample	Composition of the fumed oxide carrier, %wt.			m_{Me} in mixed NiO/Fe_xO_y/carrier, g per 1 g of fumed oxide		Calculated ratio of Ni and Fe (mmol per 1 g of fumed oxide carrier)	
	SiO_2	Al_2O_3	TiO_2	Ni	Fe	Ni	Fe
$NiO/Fe_xO_y/Al_2O_3$	-	100	-	0.102	0.026	1.74	0.47
$NiO/Fe_xO_y/SiO_2$	100	-	-	0.102	0.026	1.74	0.47
$NiO/Fe_xO_y/AST1$	10	89	1	0.102	0.026	1.74	0.47
$NiO/Fe_xO_y/SA96$	4	96	-	0.102	0.026	1.74	0.47

2.2. Methods

2.2.1. Textural characterization

To analyze the textural characteristics of NiO/Fe_xO_y/fumed oxide nanocomposites, low-temperature (77.4 K) nitrogen adsorption–desorption isotherms were recorded using a Micromeritics ASAP 2405N adsorption analyzer. The samples were degassed at 110 °C for 2 h in a vacuum chamber. The values of the specific surface area (SSA, S_{BET}) were calculated according to the standard BET method (Gregg and Sing, 1982). The total pore volume V_p was evaluated by converting the volume of adsorbed nitrogen at p/p_0 = 0.98 – 0.99 (p and p_0 denote the equilibrium and saturation pressures of nitrogen at 77.4 K, respectively) to the volume of liquid nitrogen per gram of adsorbent. The nitrogen desorption data were used to compute the pore size distributions (PSD_S, differential $f_V \sim dV_p/dR$ and $f_S \sim dS/dR$) using a self-consistent regularization (SCR) procedure under non-negativity condition ($f_V \geq 0$ at any pore radius R) at a fixed regularization parameter $\alpha = 0.01$ with voids (V) between spherical nonporous nanoparticles

packed in random aggregates (V/SCR model) (Gun'ko, 2014). The differential PSD_S with respect to pore volume $f_V \sim dV/dR$, $\int f_V dR \sim V_p$ were re-calculated to incremental PSD (IPSD) at $\Phi_V(R_i) = (f_V(R_{i+1}) + f_V(R_i))(R_{i+1} - R_i)/2$ at $\sum\Phi_V(R_i) = V_p$. The f_V and f_S functions were also used to calculate contributions of nanopores (V_{nano} and S_{nano} at 0.35 nm < R < 1 nm), mesopores (V_{meso} and S_{meso} at 1 nm < R < 25 nm), and macropores (V_{macro} and S_{macro} at 25 nm < R < 100 nm).

2.2.2. Scanning electron microscopy (SEM)

The surface morphology of composites was analyzed using field emission Scanning Electron Microscopy employing a QuantaTM 3D FEG (FEI, USA) apparatus operating at the voltage of 30 kV.

2.2.3. Particle size distribution in aqueous medium

Particle size distributions (PaSD) of nanocomposites in the aqueous medium were studied with a Zetasizer Nano ZS (Malvern Instruments) apparatus using a universal dip cell ZEN1002 (Malvern Instruments) and a wavelength λ = 633 nm and a scattering angle of 13 and 176° at 298 K. The particle size determination accuracy and repeatability are ±1-2%. Refractive index and absorption were 1.59 and 0.01, correspondingly. The samples for the PaSD measurement were prepared as follows: 0.1 wt.% suspension of a composite in distilled water was sonicated for 3 min at 22 kHz using an ultrasonic disperser UZDN-A (500 W). The suspensions were equilibrated for 24 h, and the PaSD were measured. The information obtained from the experiment on quasi-elastic light scattering is the distribution of light scattering intensity (PaDSI) from objects by diffuse broadening. However, it is not the intensity distribution itself that is of interest, but the associated particle size distribution related to number ($PaDS_N$), or molecular weight distribution ($PaDS_M$), or related volume ($PaDS_V$). A collation of this information allows us to comprehensively describe the structure of nanocomposite suspensions. The transition from (PaDSI) to these familiar characteristics of a polydisperse system requires the involvement of model ideas about the structure of the diffusers. To carry out the measurements and process the results obtained, the computer program of the Malvern Instruments Company was used, which assumes that the particles are spherical.

2.2.4. X-ray powder diffraction

XRD patterns were recorded at room temperature using a DRON-3M diffractometer (Burevestnik, St.-Petersburg, Russia) with CuK_α (λ = 0.15418 nm) radiation and a Ni filter in the 2θ range from 5° to 90°. The average sizes of nanocrystallites (D_{cr}) were estimated according to the Scherrer equation (Jenkins and Snyder 1996). Crystalline structure of samples was analyzed using the JCPDS Database (International Center for Diffraction Data, PA, 2001).

3. Results and discussion

3.1. Textural characterization

The shape of the nitrogen adsorption-desorption isotherms (Fig. 1) can be attributed to type II with hysteresis loop H3 of the IUPAC classification (Sing et al., 2001; Thommes et al., 2001) indicating the textural porosity of aggregates of nonporous nanoparticles. The presence of such form of hysteresis loop indicates dominant contribution of mesopores, that filled by nitrogen during the measurements. The textural characteristics of oxide nanocomposites calculated from the nitrogen adsorption isotherms are given in Table 1.

The BET surface area and pore volume of composites (Table 1) depend on the values of spesific surface area (SSA) of the fumed oxide carriers. In general, after modification of fumed oxides with mixed oxide of nickel and iron, the SSA value of the composite changes insignificantly. There is a tendency to a slight decrease in the S_{BET} values of composites that is observed for almost all carriers, with exception for AST1, for which a slight increase in the SSA value was observed. The total pore volume and volume of mesopores are typically greater for the composites than for the initial fumed oxides due to compaction of the powders under the synthesis. The compaction results in a decrease in the empty volume ($V_{em} = 1/\rho_b - 1/\rho_0$, where ρ_b and ρ_0 denote the bulk and true densities of the powder materials)

in the powders since the bulk density increases. However, the volume of mesopores can be increased due to closer location of nonporous nanoparticles in their aggregates and agglomerates of aggregates (Gun'ko et al., 2016). All synthesized composites demonstrate pore size distributions with a predominant contribution from mesopores (Table 1, Fig. 2).

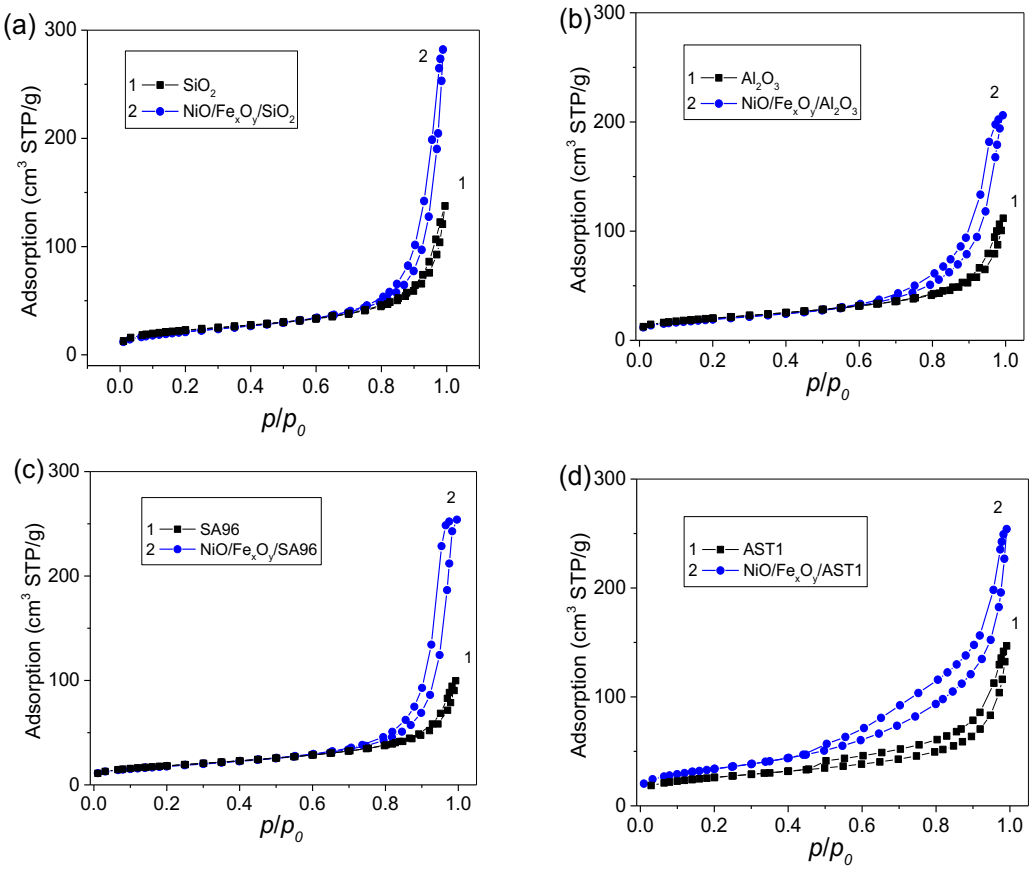

Fig. 1. Nitrogen adsorption–desorption isotherms for initial fumed oxides and nanocomposites

The pore size distribution functions (Fig. 2) confirm the conclusion based on the isotherm shapes (Fig. 1) that the composites are mainly mesoporous, since contributions of micropores and macropores are small (Table 1). The first peak is due to really small contribution of nanopores at R < 1 nm. However, the second one is due to ineffective adsorption of nitrogen in macropores because the interactions of nitrogen molecules with large distant NPNP are very weak. Therefore, being nitrogen molecules in bound fluid is not predominant in broad macropores. The first peak of the PSD (Fig. 2) corresponds to narrow voids between nanoparticles closely located in the same aggregates. Broader voids can be present between distant NPNP in the same aggregate or neighboring aggregates.

The contribution of macropores increases (Fig. 2) for samples $NiO/Fe_xO_y/SiO_2$ and remains almost unchanged for while $NiO/Fe_xO_y/Al_2O_3$ and NiO/Fe_xO_y/AST1, and decreases for NiO/Fe_xO_y/SA96 due to the filling of interparticle voids in SA96 aggregates with NiO/Fe_xO_y nanoparticles. The total pore volume V_p and the volume of mesopores increases for all composites compared to the initial fumed oxides (Table 1). As a result, the changes in pore volume depend on the type of support, features of the formation of the second phase, decrease in the void volume in the aggregates of nanoparticles, and the difference in the true density of the deposited oxide particles and fumed oxide carriers that is minimal for silica.

3.2. Scanning electron microscopy

SEM images of NiO/Fe_xO_y/fumed oxide nanocomposites (Figs. 3 and 4) show the formation of NiO/Fe_xO_y particles at a nanocarriers surface. The aggregated structures of grafted oxides of 20 to 30 nm in size were well observed for $NiO/Fe_xO_y/SiO_2$ and 10-15 nm in size for $NiO/Fe_xO_y/Al_2O_3$ (Fig. 3)

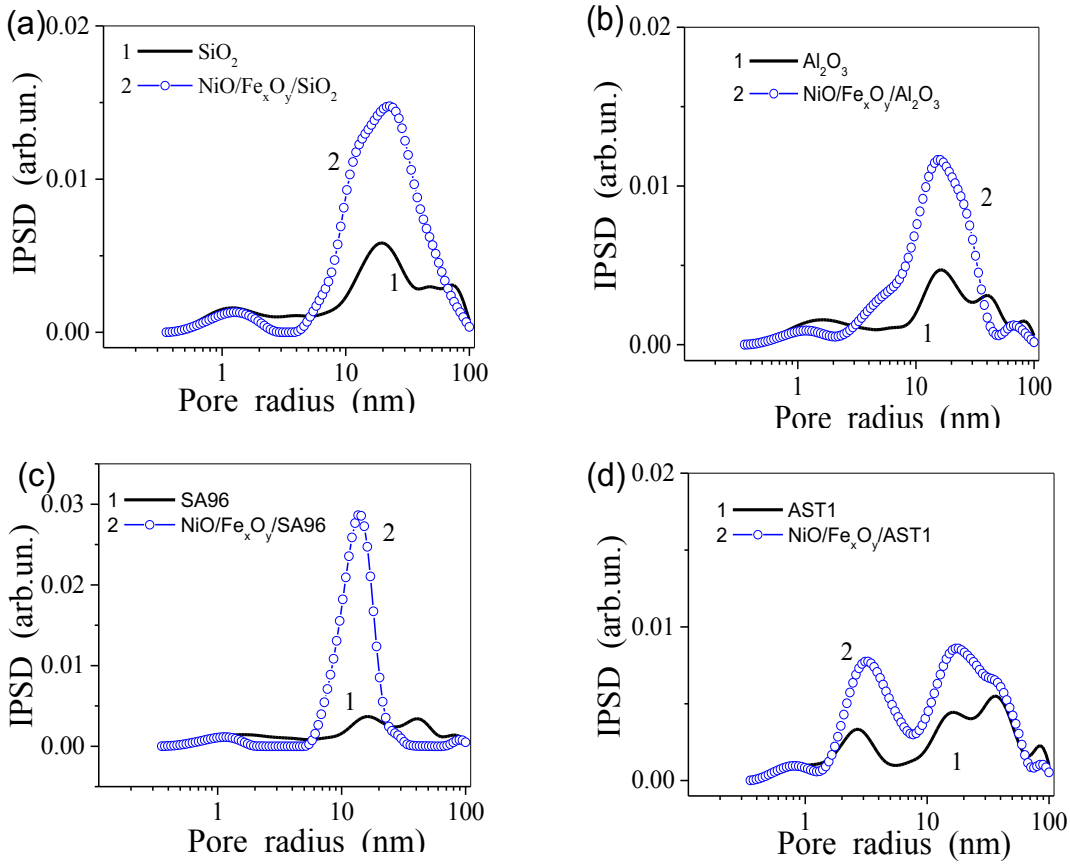

Fig. 2. Incremental pore size distributions for initial fumed oxides and nanocomposites

and $NiO/Fe_xO_y/SA96$ and $NiO/Fe_xO_y/AST1$ (Fig. 4). As a whole, the composites look like more compacted than the initial fumed nanocarriers (Figs. 3 and 4).

According to SEM/EDX data, it can be seen that in the case of mixed fumed oxides as carriers, the surface content of aluminum is significantly reduced. This indicates that the synthesis of the deposited oxide phase occurs mainly in areas corresponding to Al_2O_3 patches or having a solid solution structure with bridge-type Al-O-Si or Al-O-Ti centers, which is especially noticeable for AST1 with a decrease in the Al surface concentration up to 39%. The Ni and Fe surface concentrations insignificantly depend on the carrier nature and it varies for Ni from 12.4-12.7 over individual carriers (Al_2O_3 and SiO_2) and 13.2-13.5 over mixed carriers (SA96 and AST1) and 3.6-4.1 for Fe. The average Ni/Fe wt.% ratio calculated from the SEM/EDX data for all nanocomposites (Table 3) is very close to the given values upon the synthesis (Ni : Fe = 4 : 1).

Table 3. SEM/EDX data

	Si	**Al**	**Ti**	**O**	**Ni**	**Fe**
	wt.%	wt.%	wt.%	wt.%	wt.%	wt.%
SiO_2	36.9	-	-	63.1	-	-
$NiO/Fe_xO_y/SiO_2$	33.1	-	-	51.1	12.4	3.9
Al_2O_3	-	50.8	-	49.2	-	-
$NiO/Fe_xO_y/Al_2O_3$	-	37.5	-	46.3	12.7	3.6
SA96	0.06	48.1	-	51.9	-	-
$NiO/Fe_xO_y/SA96$	0.69	35.4	-	46.7	13.5	3.8
AST1	5.3	41.8	1.3	51.6	-	-
$NiO/Fe_xO_y/AST1$	10.7	25.6	0.7	45.3	13.2	4.1

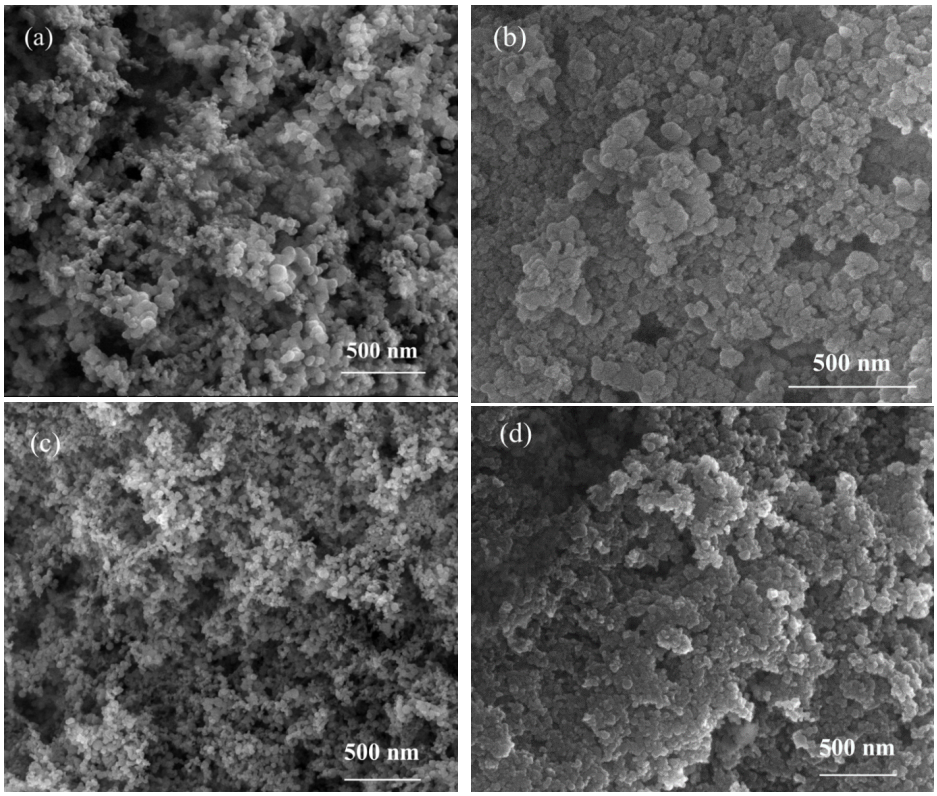

Fig. 3. SEM images of initial nanocarriers SiO_2 (a), Al_2O_3 (c), and $NiO/Fe_xO_y/SiO_2$ (b), $NiO/Fe_xO_y/Al_2O_3$ (d) nanocomposites

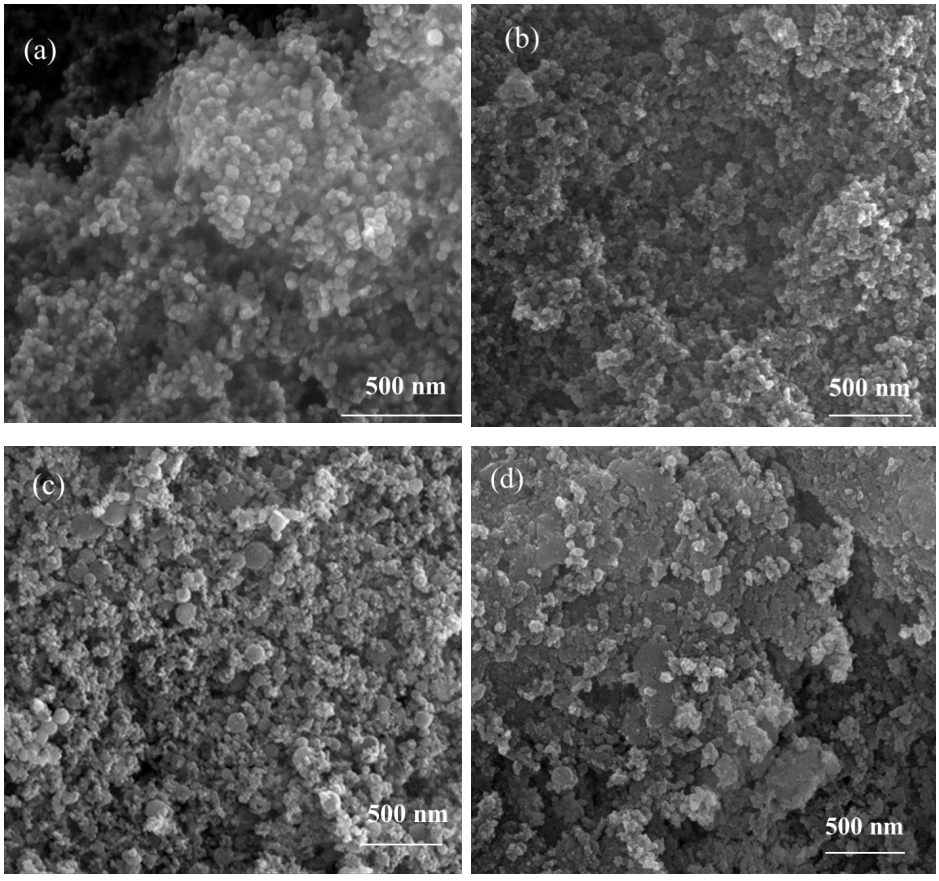

Fig. 4. SEM images of initial nanocarriers SA96 (a), AST1 (c) and $NiO/Fe_xO_y/SA96$ (b) and $NiO/Fe_xO_y/AST1$ (d) nanocomposites

3.3. X-ray powder diffraction analysis

XRD patterns of NiO/Fe_xO_y/fumed oxide nanocomposites (Fig. 5) show the presence of nickel oxide crystallites for all samples. Diffraction peaks at 2θ = 37.35, 43.4, 63.1, and 75.55° can be assigned to the (111), (200), (220) and (311) planes of NiO (Andreas et al., 2001). The crystallite sizes of NiO particles calculated the line at 43.4° using Scherrer equation (Jenkins and Snyder 1996) are listed in Table 4.

The crystalline peak of iron oxide was identified only for the $NiO/Fe_xO_y/SiO_2$ composite on the background of the amorphous SiO_2 matrix. In the case of composites based on carriers with crystalline phases (Al_2O_3, SA96, and AST1), diffraction lines of iron oxide are weak and implemented into a common pattern of nanocomposites. It is obvious that iron oxide is formed on the surface of the carriers in the form of a nanosized phase.

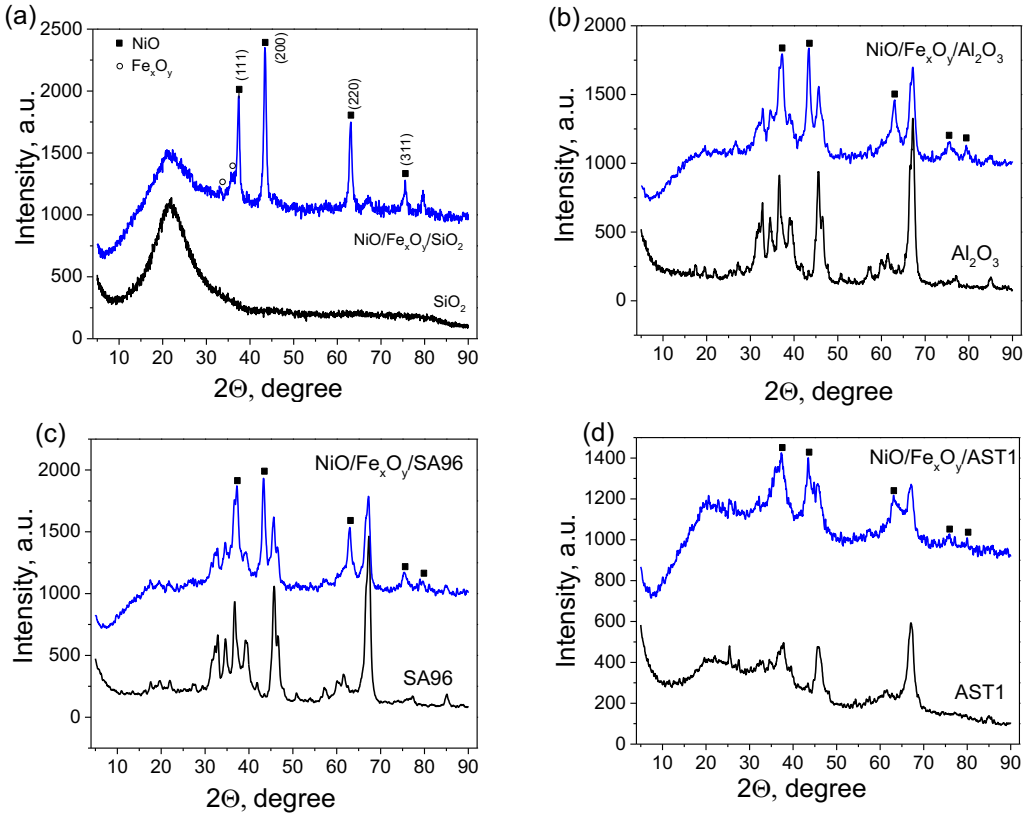

Fig. 5. XRD patterns of NiO/Fe_xO_y/fumed oxides nanocomposites

Table 4. The size of NiO crystallites formed on the surface of nanocomposites

Sample	2θ, deg.	*D*, nm
$NiO/Fe_xO_y/SiO_2$	43.4	23
$NiO/Fe_xO_y/Al_2O_3$	43.4	14
NiO/Fe_xO_y/SA96	43.4	18
NiO/Fe_xO_y/AST1	43.4	7

3.4. Particle size distribution in aqueous medium

The quasi-elastic light scattering (QELS) method allows determining the particle size distribution (PaSD) in the aqueous medium. The results of measurements for the synthesized samples of mixed oxides are presented in the form of the dependence of the particle size distribution for their number $PaSD_N$ and volume $PaSD_V$ (Fig. 6). The modification of silica with Ni and Fe oxides leads to an increase

in the particle sizes due to the formation of the second oxide phase and enhanced aggregation during the synthesis. The degree of aggregation/agglomeration depends on the characteristics of nanoparticles and their interactions in the dispersion media. The initial fumed oxides (SiO_2, Al_2O_3, SA96) are characterized by nearly monomodal PaSD related to the particle numbers with a maximum at 100-110 nm (Fig. 6, curve 1), with exception of AST1 having more complicate particulate morphology.

The $PaSD_N$ of the composites are mono- or bimodal (Fig. 6) and three peaks are observed for $PaSD_V$ (Fig. 6): aggregates ~90 and ~430 nm (SiO_2) and large agglomerates > 5.5 μm are presence in aqueous dispersion of composites after ultrasonic treatment. It should be noted that although for the composites

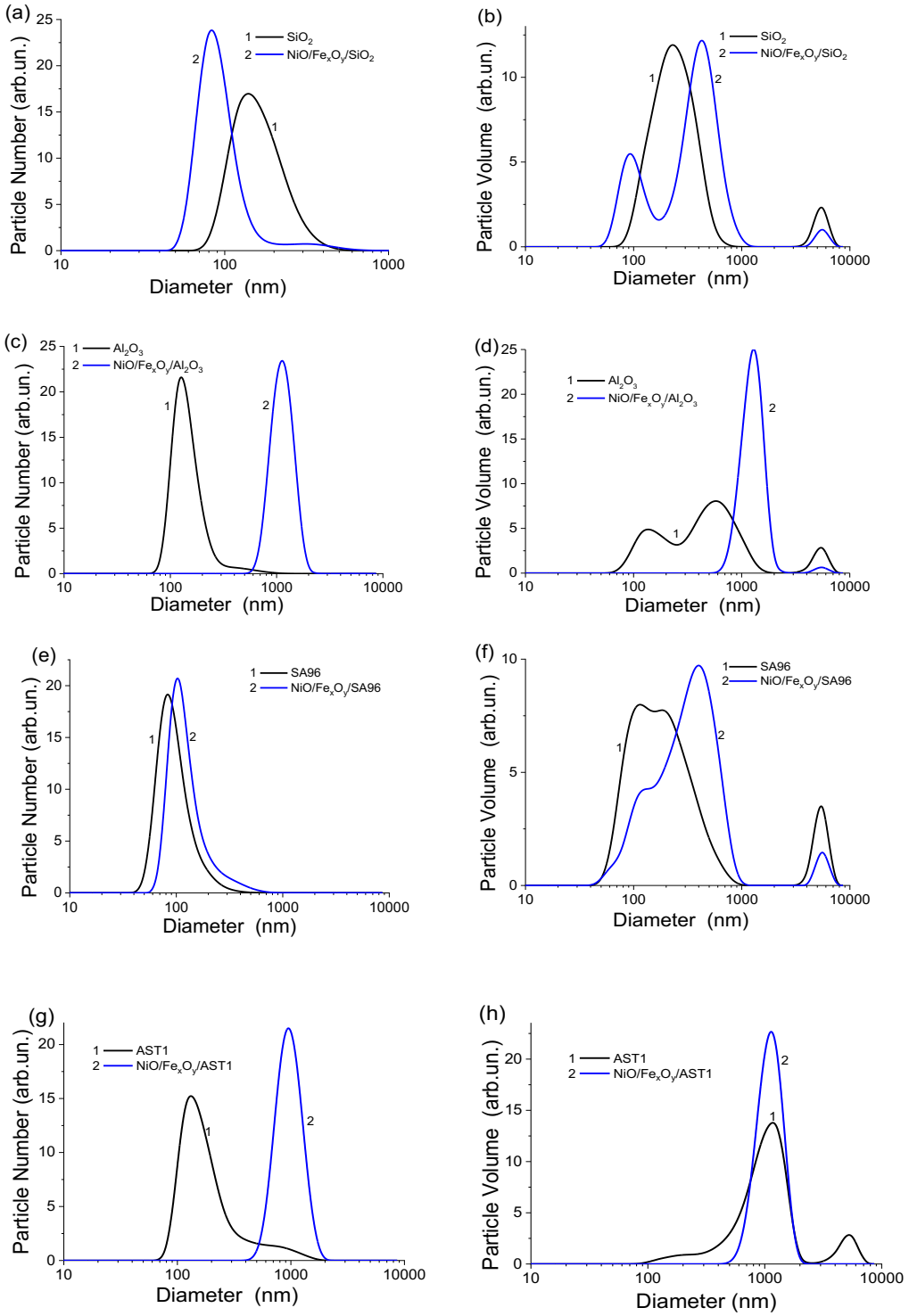

Fig. 6. PaSD related to number (a, c, e, and g) and volume (b, d, f,and h) for initial fumed nanocarriers and nanocomposites with NiO/Fe_xO_y after sonication (6 min) of the aqueous dispersions (C = 0.1 wt.%)

$PaSD_N$ shows a maximum at 85-103 nm for SiO_2 and SA96 carrier, i.e., the number of small secondary particles of ~100 nm is more than the number of large aggregates (>1μm). However, according to $PaSD_V$, the volume of aggregates > 1 μm for these composites is much higher than that for initial nanocarriers. The PaSD for Ni- and Fe-containing composites supported on Al_2O_3 and AST1 are characterized by the presence of aggregates and agglomerates of larger sizes (~ 1.1-1.3 and 5.5 μm). The aggregates less than 1 μm in size are not observed in the dispersion. This indicates stronger bonds of the deposited guest oxide with the support.

4. Conclusions

Novel Ni_xO_y/Fe_xO_y/fumed oxide nanocomposites were synthesized by thermooxidation of metal salts adsorbed onto the individual and complex fumed nanooxides. The effects of the support structure were analyzed with respect to the formation of the deposited phases. The phase composition and average sizes of crystallites determined from the XRD data show that NiO phase in NiO/Fe_xO_y/fumed oxide nanocomposites includes crystallites of 7-23 nm in diameter while the iron oxide reflexes are not practically identified. According to XRD and SEM/EDX data, the use of ternary oxide $Al_2O_3/SiO_2/TiO_2$ as a carrier leads to the formation of the smallest crystallites of NiO/Fe_xO_y (7 nm) due to a large number of active surface sites served as centers of the new deposited phase crystallization. The specific surface area of the composites changes insignificantly when the phase NiO/Fe_xO_y was deposited on the support. The incremental pore size distribution functions show predominantly the mesoporosity of nanocomposites, the volume of mesopores increases significantly in comparison to the initial fumed oxides. According to QELS data for aqueous dispersions of the synthesized nanocomposites, small aggregates with several nanoparticles of 100 nm in size, large aggregates up to ~1 μm, and agglomerates up to 5.5 μm are observed. There is a general tendency in increasing sizes of aggregates due to the modification of nanocarriers with the deposited NiO/Fe_xO_y.

Acknowledgments

The authors are grateful to Professor V.M. Gun'ko for the developed and provided program for calculating the pore size distribution.

References

ARANDIYAN, H.R., PARVARI, M, 2009. *Studies on mixed metal oxides solid solutions as heterogeneous catalysts.* Braz. J. Chem. Eng., 26, 63-74.

ANDERSSON, M.P., BLIGAARD, T., KUSTOV, A., LARSEN, K.E., GREELEY, J., JOHANNESSEN, T., CHRISTENSEN, C.H., NØRSKOV, J.K., 2006. *Toward computational screening in heterogeneous catalysis: Pareto-optimal methanation catalysts.* J. Catal., 239, 2, 501-506.

BEACH, E., BROWN, S., SHQAU, K., MOTTERN, M., WARCHOL, Z., MORRIS, P., 2008. *Solvothermal synthesis of nanostructured NiO, ZnO and Co_3O_4 microspheres.* Mater. Lett. 62, p. 1957–1960.

BEACH, E.R., SHQAU, K., BROWN, S.E., ROZEVELD, S.J., MORRIS, P.A., 2009. *Solvothermal synthesis of crystalline nickel oxide nanoparticles*. Mater. Chem. Phys., V.115(1), 371-377.

BOGATYREV, V.M., GUN'KO, V.M., GALABURDA, M.V., BORYSENKO, M.V., POKROVSKIY, V.A., ORANSKA, O.I., POLSHIN, E.V., LEBODA, R., SKUBISZEWSKA-ZIĘBA, J. 2009. *Synthesis and characterization of Fe_2O_3/SiO_2 nanocomposites*. J. Colloid and Interface Science, 338, 376-388.

CHOWDHURY, A.N., RAHIM, A., FERDOSI, Y. J., AZAM, MD. SH., HOSSAIN, M. M. 2010, *Cobalt–nickel mixed oxide surface: A promising adsorbent for the removal of PR dye from water.* Applied Surface Science, 256, 3718–3724.

DENG, X.Y., CHEN, Z., 2004. *Preparation of nano-NiO by ammonia precipitation and reaction in solution and competitive balance*, Mater. Lett. 58, 276, 276–280.

DIAS, Y.R., PEREZ-LOPEZ, O.W. 2021. *CO_2 conversion to methane using Ni/SiO_2 catalysts promoted by Fe, Co and Zn.* Journal of Environmental Chemical Engineering, 9, 1, 104629

EBERT, D.Y., DOROFEEVA, N.V., SAVEL'EVA, A.S., KHARLAMOVA, T.S., SALAEV, M.A., SVETLICHNYI, V.A., MAGAEV, O.V., VODYANKINA, O.V. 2018. *Silica-supported Fe-Mo-O catalysts for selective oxidation of propylene glycol*. Catalysis Today.

GALABURDA, M.V., KLONOS, P., GUN'KO, V.M., BOGATYROV, V.M., BORYSENKO, M.V., PISSIS, P., 2014. *Dielectric properties and thermal destruction of poly(dimethylsiloxane)/Fe_2O_3/SiO_2 nanocomposites.* Applied Surface Science, 305, 67-76.

GAOA, Y., DOUA, L., ZHANGA, SH., JIEPANC, L.Z., HAO, X.H., OSTRIKOVD, S.K., SHAOABE, T., 2021. *Coupling bimetallic Ni-Fe catalysts and nanosecond pulsed plasma for synergistic low-temperature CO_2 methanation.* Chemical Engineering Journal, V. 420, Part 2, 127693.

GREGG, S.J, SING, K.S.W. 1982 Adsorption, Surface Area and Porosity (Academic Press, London)

GONCHARUK, O., SHIPUL, O., DYACHENKO, A., ISCHENKO, O., ANDRIYKO, L., MARYNIN, A., PAKHLOV, E. ORANSKA, O., BORYSENKO M. 2019. *Silica-supported Ni and Co nanooxides: Colloidal properties and interactions with polar and nonpolar liquids.* Journal of molecular liquids. V. 285, P. 397-402.

GUN'KO, V.M., BLITZ, J.P., BANDARANAYAKE, B., PAKHLOV, E.M., ZARKO, V.I., SULYM, I.YA., KULYK, K.S., GALABURDA, M.V., BOGATYREV, V.M., ORANSKA, O.I., BORYSENKO, M.V., LEBODA, R., SKUBISZEWSKA-ZIĘBA, J., JANUSZ, W., 2012. *Structural characteristics of mixed oxides MOx/SiO_2 affecting photocatalytic decomposition of methylene blue.* Applied Surface Science, 258, 6288-6296.

GUN'KO, V.M. 2014. *Composite materials: textural characteristics.* Appl Surf Sci. 307 444

GUN'KO, V.M., TUROV, V.V., ZARKO, V.I., GONCHARUK, O.V., PAKHLOV, E.M., SKUBISZEWSKA-ZIĘBA, J., BLITZ, J.P. *Interfacial phenomena at a surface of individual and complex fumed nanooxides*, Adv. Colloid Interface Sci. 235 (2016) 108–189.

HAN, D.Y., YANG, H.Y., SHEN, C.B., ZHOU, X., WANG, F.H. 2004. *Synthesis and size control of NiO nanoparticles by water-in-oil microemulsion,* Powder Technology, 147(1–3), 113-11.

IRFAN, M., DOGAN, N., BINGOLBALI, A., ALIEW, F. 2021. *Synthesis and characterization of $NiFe_2O_4$ magnetic nanoparticles with different coating materials for magnetic particle imaging (MPI)* Journal of Magnetism and Magnetic Materials, 537, 168150.

The Chemistry of Silica. Solubility, Polymerization, Colloid and Surface Properties, and Biochemistry. ILER, VON R. K. John Wiley and Sons, Chichester 1979. XXIV, 886 p

JIANFEN, L.I., RONG, YAN, B.O., XIAO, DAVID, T.E.E, LIANG, LIJUAN, D.U., 2008. *Development of Nano-NiO/Al_2O_3 Catalyst to be Used for Tar Removal in Biomass Gasification.* Environ. Sci. Technol., 42, 16, 6224–6229.

JENKINS R., SNYDER R.L. 1996. Introduction to X-ray Powder Diffractometry (New York: Wiley).

JCPDS Database, International Center for Diffraction Data, PA 2001 Available at: http://www.icdd.com

KLONOS, P., PISSIS, P., GUN'KO, V.M., KYRITSIS, A., GUZENKO, N.V., PAKHLOV, E.M., ZARKO, V.I., JANUSZ, W., SKUBISZEWSKA-ZIĘBA, J., LEBODA, R., 2010. *Interaction of poly(ethylene glycol) with fumed silica and alumina/silica/titania.* Colloids and Surfaces A: Physicochemical and Engineering Aspects, 360, 220-231.

KLONOS, P., KULYK, K., BORYSENKO, M.V., GUN'KO, V.M., KYRITSIS, A., PISSIS, P., 2016. *Effects of Molecular Weight below the Entanglement Threshold on Interfacial Nanoparticles/Polymer Dynamics*, Macromolecules, 49, 9457–9473.

LAI, T.L., SHUB, Y.Y., HUANG, G.L., LEE, C.C., WANG, C.B., 2008. *Microwave-assisted and liquid oxidation combination techniques for the preparation of nickel oxide nanoparticles. J.* Alloys Compd. 450, 318.

LEINEWEBER, A., JACOBS, H., HULL, S., 2001. *Ordering of Nitrogen in Nickel Nitride Ni_3N Determined by Neutron Diffraction*. Inorganic Chemistry 40, 5818-5822.

LENGGOROA, I.W., ITOH, Y., IID, N. , OKUYAMA K., 2003. *Control of size and morphology in NiO particles prepared by a low-pressure spray pyrolysis*. Mater. Res. Bull. 38, 1819.

LYSOV, D.V., KUZNETSOV, D.V., YUDIN, A.G., MURATOV, D.S., LEVINA, V.V., RYZHONKOV, D.I., 2010, *Preparation of nickel oxide nanostructured powders under the action of ultrasound*. Nanotechnologies in Russia 5, 493.

Malvern Instruments [homepage on the Internet] 2017. Available at: https://www.malvern.com

MASHKURI, A., SALJOOQI, A., TOHIDIYAN, Z. 2017. *Nano clay Ni/NiO nanocomposite new sorbent for separation and preconcentration dibenzothiophene from crude prior to UVevis spectrophotometery determination*, Analytical Chemistry Research, 12, 47-51.

MAHMOUD, A.M., IBRAHIM, F.A., SEHAM A., YOUSSEF, S.N.A. 2015. *Adsorption of heavy metal ion from aqueous solution by nickel oxide nanocatalyst prepared by different methods*, Egyptian Journal of Petroleum, 24, 1, 27-35.

MESHKINI FAR R., ISHCHENKO O.V., DYACHENKO A.G., BIEDA O., GAIDAI S., LISNYAK V. 2018 *CO_2 hydrogenation into CH_4 over Ni–Fe catalysts*. Functional Materials Letters. V.11, N.3, 1850057.

MIAO, G., ZAN, Y., SUN, Y., WANG, H., LI, SH., LIU, CH., LI, SH., KONG, L., SUN, Y., 2018. *Mn-promoted hydrogenation of microalgae (Chlorococcum sp.) to 1,2-propanediol and ethylene glycol over Ni-ZnO catalysts*. Applied Catalysis A: General, 565, 34-45.

PALANISAMY, P., RAICHUR, A.M. 2009. *Synthesis of spherical NiO nanoparticles through a novel biosurfactant mediated emulsion technique*, Mater. Sci. Eng. C, 29(1), 199-204.

RADWAN, N.R.E., SAMY EL-SHALL, M., SAMY, EL-SHALL, M., HASSAN, M., HASSAN, A., HASSAN, M., HASSAN., A., 2007. *Synthesis and characterization of nanoparticle Co_3O_4, CuO and NiO catalysts prepared by physical and chemical methods to minimize air pollution,* Applied Catalysis A General, 331(1), 8-18.

RAVINDHRANATH, K., RAMAMOORTY, M. 2017. *Nickel Based Nano Particles as Adsorbents in Water Purification Methods*. A Review, Oriental Journal of Chemistry, 33, 4, 1603-1613.

PINES, H., HAAG W.O. *Alumina: Catalyst and Support. I. Alumina, its Intrinsic Acidity and Catalytic Activity*, J. Am. Chem. Soc. 1960, 82, 10, 2471–2483.

PULIMI, V.R.R., JEEVANANDAM, P., 2009. *The effect of anion on the magnetic properties of nanocrystalline NiO synthesized by homogeneous precipitation* J. Magn. Magn. Mater., 321, 17, 2556-2562.

SATO, A.G., VOLANTI, D.P., MEIRA, D.M., DAMYANOVA S., LONGO, E. J.M.C. 2013. *Bueno Effect of the ZrO_2 phase on the structure and behavior of supported Cu catalysts for ethanol conversion.* Journal of Catalysis 307, 1–17.

SAFDARI, T., 2020. *Iron-nickel oxide: A promising strategy for water oxidation*. New J. Chem., 44, 1517-1523.

SCHMIDT, G. Nanoparticles: From Theory to Application, VCH, Weinheim, 2004.

Synthesis of Inorganic Nanomaterials. Advances and Key Technologies / ed. S.M. Bhagyaraj et al. India: Elsevier, 2018. P. 19–57.

SING, K.S.W, EVERETT, D.H, HAUL RAW, MOSCOU L, PIEROTI R.A., ROUQUEROL J., SIEMIENIEWSKA T., 1985. *Reporting Physisorption Data for Gas/Solid Systems with Special Reference to the Determination of Surface Area and Porosity*. Pure Appl Chem, 57, 603.

SULYM, I., GONCHARUK, O., STERNIK, D., SKWAREK, E., DERYLO-MARCZEWSKA, A., JANUSZ, W., GUN'KO, V.M. 2016. *Silica-Supported Titania-Zirconia Nanocomposites: Structural and Morphological Characteristics in Different Media*. Nanoscale Res Lett. Dec, 11(1), 111.

SULYM, I., GONCHARUK, O., SKWAREK, E., STERNIK, D., BORYSENKO, M.V., DERYLO-MARCZEWSKA, A., JANUSZ, W., GUN'KO, V.M. 2015. *Silica-supported ceria-zirconia and titania-zirconia nanocomposites: Structural characteristics and electrosurface properties.* Colloids and Surfaces A: Physicochemical and Engineering Aspects, 482, 631-638

SULYM, I., STERNIK, D., OLEKSENKO, L., LUTSENKO, L., BORYSENKO, M., DERYLO-MARCZEWSKA, A. 2016. *Highly dispersed silica-supported ceria–zirconia nanocomposites*: *Preparation and characterization*. Surfaces and Interfaces, 5, 8-14.

SURCA, A., OREL, B., PIHLAR, B., BUKOVEC, P., 1996. *Optical, spectroelectrochemical and structural properties of sol-gel derived Ni-oxide electrochromic film*. J. Electroanal. Chem. 408, 83.

TANAKA, H., BOULINGUIEZ, M., VRINAT, M., 1996. *Hydrodesulfurization of thiophene, dibenzothiophene and gas oil on various Co-Mo/TiO_2-Al_2O_3 catalysts*. Catal Today, 29, 209–213.

TEOH, L.G., LI K.-D. 2012. Synthesis and Characterization of NiO Nanoparticles by Sol-Gel Method. Materials Transactions, V. 53 (12), pp. 2135-2140.

THOMMES M, KANEKO K, NEIMARK AV, OLIVIER JP, RODRIGUEZ-REINOSO F, ROUQUEROL J, SING KSW, 2015 Pure Appl. Chem.; IUPAC Technical Report; Physisorption of gases, with special reference to the evaluation of surface area and pore size distribution (IUPAC Technical Report).

TAKEI, T., IGUCHI, N., HARUTA M. 2011. *Support effect in the gas phase oxidation of ethanol over nanoparticulate gold catalysts*. New J. Chem., 35, 2227-2233.

TRUEBA, M., TRASATTI, S. 2005. *γ-Alumina as a Support for Catalysts: A Review of Fundamental Aspects*. Eur. J. Inorg. Chem., 3393–3403.

TEERAPAT RUTIRAWUT, WANWISA LIMPHIRAT, ASAWIN SINSARP, KRITSANU TIVAKORNSASITHORN, TOEMSAK SRIKHIRIN, TANAKORN OSOTCHAN, 2015. *Composition and Oxidation State of Cobalt- and Nickel-Iron Oxide Colloidal Nanoparticles in Liquid Phase*, Advanced Materials Research 1103, 21-27.

THOTA, S., KUMAR, J., 2007, *Sol–gel synthesis and anomalous magnetic behaviour of NiO nanoparticles*. J. Phys. Chem. Solids 68, 1951.

WANG, Y.A., ZHU, J., YANG, X., LU, L., WANG, X., 2005. *Preparation of NiO nanoparticles and their catalytic activity in the thermal decomposition of ammonium perchlorate*, Thermochimica Acta, 437, 1, 106-109.

WANG, W.N., ITOH, Y., LENGGORO, I.W., OKUYAMA, K., 2004. *Nickel and Nickel Oxide Nanoparticles Prepared from Nickel Nitrate Hexahydrate by a Low Pressure Spray Pyrolysis*. Mater. Sci. Eng. B 111, 69.

WEI, W., JIANG, X., LU, L., YANG, X., WANG, X, 2009. *Study on the catalytic effect of NiO nanoparticles on the thermal decomposition of TEGDN/NC propellant,* J. Hazard Mater. 168, 2-3, 838-42.

WISNIEWSKA, M., NOWICKI, P., BOGATYROV, V.M., NOSAL-WIERCINSKA, A., PIETRZAK, R., 2016. *Comparison of adsorption properties of Mg_xO_y-SiO_2 and Zn_xO_y-SiO_2 in the mixed oxide-poly (vinyl alcohol) system*. Colloids and Surfaces A: Physicochem. Eng. Aspects, 492, 12–18.

WU, Y., HE, Y., WU, T., CHEN, T., WENG, W., WAN, H. 2007. *Influence of some parameters on the synthesis of nanosized NiO material by modified sol–gel method*. Mater. Lett. 61, 3174.

ZHANG, Y., RIMAL, G., TANG, J., DAI Q. 2018. *Synthesis of $NiFe_2O_4$ Nanoparticles for Energy and Environment Applications*, Mater. Res. Express, 5, 025023.